

# We are IntechOpen, the world's leading publisher of Open Access books Built by scientists, for scientists

6,900

Open access books available

186,000

International authors and editors

200M

Downloads

Our authors are among the

154

Countries delivered to

TOP 1%

most cited scientists

12.2%

Contributors from top 500 universities



WEB OF SCIENCE™

Selection of our books indexed in the Book Citation Index  
in Web of Science™ Core Collection (BKCI)

Interested in publishing with us?  
Contact [book.department@intechopen.com](mailto:book.department@intechopen.com)

Numbers displayed above are based on latest data collected.  
For more information visit [www.intechopen.com](http://www.intechopen.com)



---

# Mn-Zn Ferrite as Recycled Material Resource Based on Iron Oxide Suitable to Functional Green Devices

---

Roberto Baca

Additional information is available at the end of the chapter

<http://dx.doi.org/10.5772/intechopen.72418>

---

## Abstract

Today manufacturing stages in electronic device industry of wide-scale production can be restricted due to the high costs resulting from energy consumption, the use of organic solvents, production of hazardous intermediates, and formation of waste products leading to environmental pollution and several biological risks which damage society's ability to sustain the planet for future generations. As recycled material resource based on iron oxide, the Mn-Zn ferrite is an interesting candidate. In the last decades, this material has been manufactured by using ceramic process technologies to design magnetic devices as components useful in switching mode electronic systems. However, these processing technologies have generated negative environmental impact as emission of toxic gases and higher use of energy resources. The Mn-Zn ferrites employed in consumer electronics deteriorate the earth when its final placement as waste in landfills occurs. Then, attitudes in resource recovery should allow the recycling of the materials from electronic waste to converting those to new products; therefore, uncommon physical properties from shredding processes are available when bulk ferrites are converted to foil ferrites. This chapter provides a comprehensive study on recyclability of the Mn-Zn ferrites, exploring both structure and conduction properties in foil ferrites to use their nonlinear behavior in functional green devices.

**Keywords:** electronic waste, shredding phase, life-cycle analysis, foil ferrite, functional green device

---

## 1. Introduction

In the past, a large number of physical and chemical processes have been widely used to manufacturing the different types of electronic devices with the desired characteristics [1, 2]. Beyond the supply of raw materials during manufacturing cycles, however, the environmental and human

health impacts have restricted the wide-scale production [3, 4]. In response to those concerns, coherent procedures that enable device manufacturers to reduce or eliminate toxic substances in their designs will be a major advance toward green development.

It is well known that for the materials selection for conventional electronic devices, the primary purpose is link material and function. The latter has been achieved by focusing on selected material attributes, including mechanical, thermal, electrical, optical, and chemical properties, and processing characteristics [5]. Also, traditionally selection has been focused solely on cost; nevertheless, availability, environmental consequences of use, and recycling must also become important factors. Recycling is the transformation of waste into usable products or materials; it is sometimes referred as resources recovery which might be often more environmentally gentle than using raw materials owing to reduced energy use and elimination of hazardous gases and other pollutants [6].

The assessment of recycling potential must be based on established principles, including knowledge of the relative ease of “liberation” of the materials of interest and specific characteristics during physical separation technology and shredding in accordance with the international materials life-cycle initiative established by the United Nations Environmental Program (UNEP) and the Society for Environmental Toxicology and Chemistry (SETAC) [7]. Conversely, design of products profoundly will affect the potential recyclability of the resources they contain [8].

The chapter is focused on recovery of one useful material based on iron oxide well known as Mn-Zn ferrite extracted from unusable electronic systems. Using a scientific tool known as life-cycle assessment (LCA), which takes into account all stages of the life cycle of products or materials, including processing technology, manufacturing processes, use phase, and end-of-life routes, will deliver powerful basis to quantifying the recycling performance. Thus, researching Mn-Zn ferrites in foil shape will provide theoretical basis for open-loop recycling, converting waste materials into suitable materials in its second life.

This chapter is organized as follows. After introducing the recycling concept and their environmental advantages, it presents the Mn-Zn foil ferrites as recycled material resource explaining the source of their uncommon physical properties. Then the following sections are focused on analysis of both structure and conduction properties to functional green devices into engineering applications.

## **2. Recycled material resource: Mn-Zn ferrite**

Ferrites are ceramic, homogeneous materials composed of various oxides with iron oxide as their main constituent. Ferrites have several distinct crystal structures. However, for this chapter, only the Mn-Zn ferrites of cubic crystal structure are concerned. Mn-Zn ferrites are used for frequencies less than 2 MHz and at room temperature have a resistivity lower at  $10^5 \Omega\text{m}$  [9]. Their first practical application was as inductors used in LC filters for frequency division multiplex equipment. The combination of high resistivity and good magnetic properties made these

ferrites an excellent material for these filters operating over the 50–450 kHz frequency range. For five decades ferrite components have been employed in a widening range of applications [10]. Currently these are useful as magnetic devices into applications such as switching mode power supplies (SMPS) and lighting electronic ballasts, matching and storage devices, interference suppression, etc.

It is well known that the magnetic structure of a Mn-Zn ferrite is noncollinear in a certain range of temperatures and magnetic fields, which results from competitions between antiferromagnetic interactions of their sublattices, aligning the sublattice magnetizations antiparallel to each other, and under an external field will try to align them parallel to each other [11]. Such magnetic interactions between d ions had allow to predict magnetic properties and thus to calculate composition with structure parameters; however, dominant interaction is exchange coupling between Mn and Fe ions caused by the magneto-crystalline anisotropy. Furthermore, it has been shown that the states of Mn and Fe ions support both ferromagnetic and antiferromagnetic long-range orders [12]. At lower field conditions, bulk ferrites always are accompanied by characteristic anomalies in their physical properties, like domain structure [13]. The last indicates that the resistivity in their grain boundaries will be short-circuited due to the domain wall excitation by the applied alternating magnetic field when the frequency changes from 10 kHz to 1 MHz [14].

Mn-Zn ferrites have been manufactured by a complex composition of iron oxide ( $Fe_2O_3$ ) mixed with manganese oxide (MnO) and zinc oxide (ZnO) by using ceramic process technologies. Ceramic process can be divided into four functions: preparation of the powder, forming powder into cores, sintering cycle, and finishing stage [9, 10]. Thus, taking into account environmental impacts, the use of energy resources, etc., efficiency in the processing technology of bulk ferrites must be studied into LCA methodology, including product manufacturing, use phase, and end of life. **Figure 1** illustrates the schematic of the life-cycle assessment methodology for bulk ferrites.

LCA methodology with the stages coverage in **Figure 1** is understood in accordance with the following. During the preparation of the powder, raw material ( $Fe_2O_3$ ) and MnO and ZnO oxides as constitutes are weighed and thoroughly mixed into a homogeneous mixture to form slurry and then mixed in a ball mill [9, 15]. After calcining process in air atmosphere at the powder temperature of approximately 1000°C, partial decomposition of the carbonates and oxide evaporation of impurities occurs.

Besides, forming powder into core geometries is done by dry pressing process, and to achieve final magnetic and mechanical characteristics in bulk ferrites, sintering cycle must be completed. This phase consists in gradual ramping up from room temperature to approximately 800°C into air atmosphere. After, the temperature is further increased to the final temperature cycle from 1000 to 1500°C, after a cool-down cycle is needed at reduced oxygen pressure. Finally, most ferrites will require some shape of finishing in accordance with their magnetic performance. Subsequently, the Mn-Zn bulk ferrites are in general employed as SMPS into product manufacture (see **Figure 1**). However, severe problems as the combination of core losses (hysteresis, eddy currents, and residual), winding losses, and failures in power semiconductor

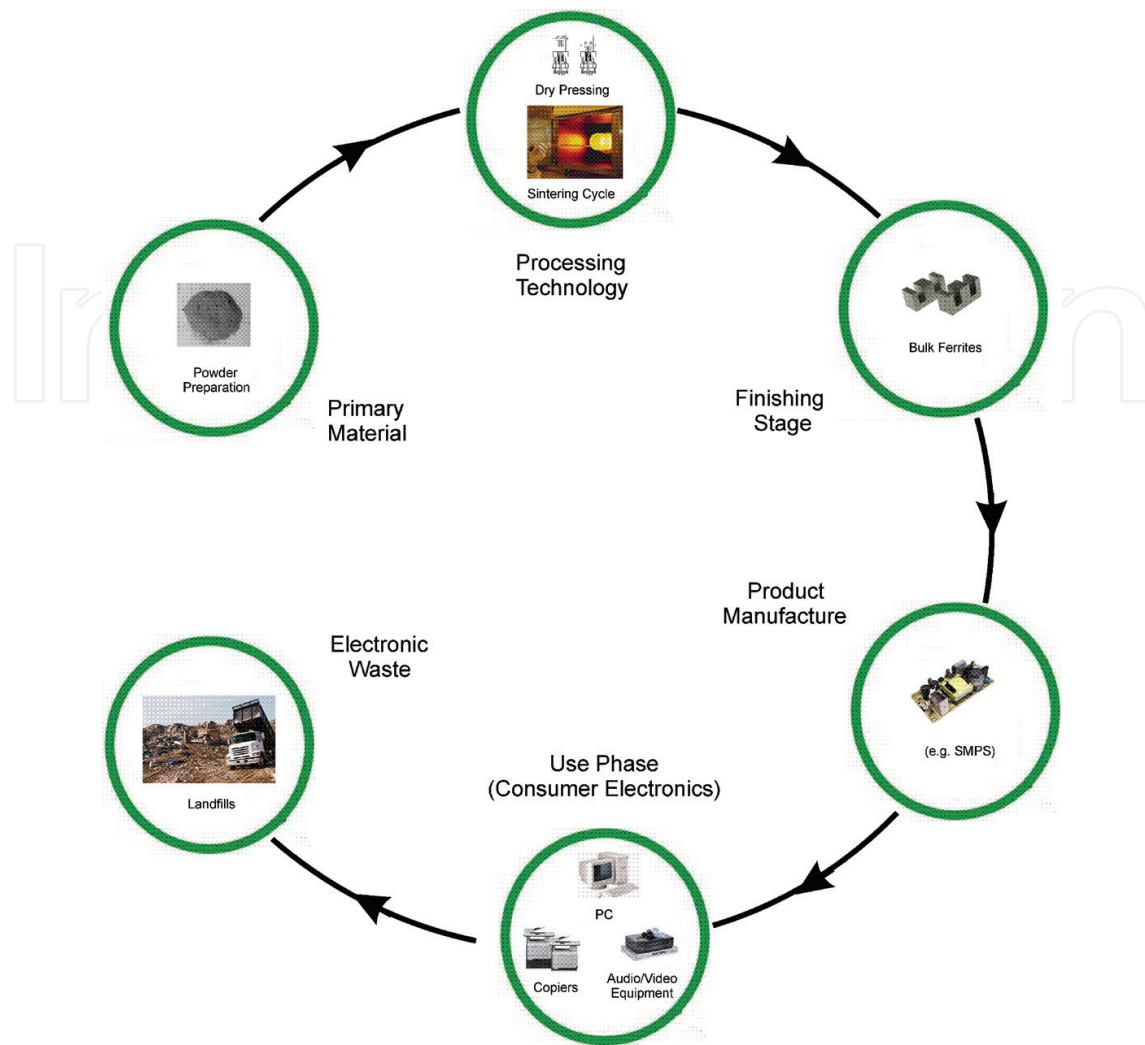


**Figure 1.** Schematic of the LCA methodology as applied to Mn-Zn bulk ferrite production including manufacturing stages and final disposal.

devices under extreme switching conditions increase losses by temperature rise resulting in thermal runaway which reduce end of life of the consumer electronics [16].

The LCA studies confirm that the processing technology of Mn-Zn bulk ferrites in their first life, including powder preparation, SMPS manufacturing, and final disposition of constituent materials, results in negative environmental impact such as emission of toxic gases during powder preparation, higher use of energy resources into sintering cycle, and electronic waste by the poorly processing technology and inadequate design of SMPS which has taken at the final placement of such these ferrites often in landfills as shown in **Figure 1**.

From earlier studies it has been identified that power losses in Mn-Zn ferrites under low-frequency excitation are close to zero, because chemical composition and oxidation degree depend on temperature like semiconductor materials; then a small grained ferrite ( $<5 \mu\text{m}$ ) with a single magnetic domain structure would be capable to drive at low frequencies ( $< 10 \text{ kHz}$ ) when bulk ferrites are converting in foil ferrites [15, 17]. Hence, such grain-reduced crystalline

structure must be evaluated using a recycling model to identify critical parameters in view of recycling performance and resource efficiency; therefore, a methodology such as Life-Cycle Green Strategy (LCGS) is proposed here. **Figure 2** illustrates the recycling model based on LCGS for recovery of Mn-Zn foil ferrites from bulk ferrites. The recycling model represents the liberation of bulk ferrites during different phases from dismantling, physical separation, and shredding phase as a function of the device-manufacture characteristics, specifically the parameters that will characterize the foil ferrites as physical dimensions to operability into an electronic signal processor (see **Figure 2**) [18].

Ferrites with E core geometry of different dimensions have been recovered from three systems: LC filter, lighting electronic ballast, and SMPS. The foil ferrites with area of  $5 \times 5 \text{ mm}^2$  and thickness of 1 mm are processed by using shredding phase. Shredding phase consists in cut into the small bulk ferrite pieces to get ease fracture pathways along each piece. The fracture strength will be depending on carefully applied mechanical stress, and when the critical fracture length occurs, uniform foil ferrites of different dimensions and thickness are attained.

The following sections in this chapter will demonstrate technological potential of foil ferrites to design suitable functional green devices. Therefore, due to the arduous task in composition

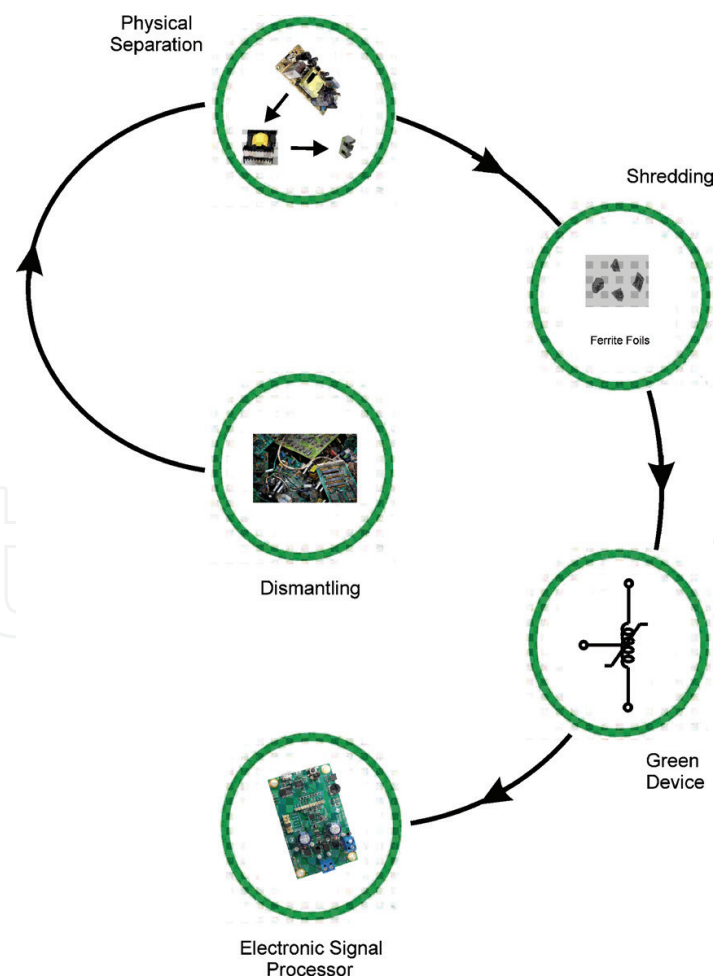


**Figure 2.** Schematic of recycling model based on LCGS as applied to recovery of foil ferrite samples.

finding of the Mn-Zn ferrites, predicting theoretically their uncommon properties is a possibility in foil ferrite analysis; then studying structure and conduction properties makes it possible to estimate their physical behavior.

### 3. Structure and conduction properties in foil ferrites

This section discusses structure and conduction properties in foil ferrites. It then reviews general capabilities of x-ray diffraction (XRD) and electrical characterization techniques for the study of foil ferrites and behavior with emphasis on knowledge of their properties. The interrelation of structure and conduction properties as a function on their magnetic ordering is the key issue in green electronic device design.

Usually, copper source with  $\text{CuK}\alpha$  radiation ( $\lambda = 0.154 \text{ nm}$ ) is employed in x-ray diffraction studies; however, features of Mn-Zn ferrites at higher wavelengths are indistinguishable. Thereby, a PANalytical x-ray diffractometer with  $\text{CoK}\alpha$  radiation ( $\lambda = 0.179 \text{ nm}$ ) is used here to obtain XRD patterns in foil ferrite samples. Cobalt source allows higher diffraction angles and peak spreads. Current-voltage measurements are performed by using a digital storage oscilloscope (Tektronix, TDS1012C) at room temperature. A function generator (Matrix, MFG-8250A) is used to produce a linear-ramp signal at low frequency ( $f = 100 \text{ Hz}$ ) with voltage scanned from  $-10 \text{ V}$  to  $10 \text{ V}$  to ensure that the magnetic saturation in the samples does not occur.

#### 3.1. X-ray diffraction analysis

**Figure 3** shows the XRD patterns of the foil ferrite samples analyzed here and labeled as FF-1, FF-2, and FF-3. These samples are polycrystalline with spinel oxide structure. Several peaks appear, which correspond to the (111), (022), (113), (004), (224), (115), (044), (026), and (335) crystallographic planes of the magnetite phase ( $\text{Fe}_3\text{O}_4$ ).

Frequently, structural defects in Mn-Zn ferrites are classified as grain boundaries, where there is a face-centered cubic lattice of oxygen ions with a unit cell consisting of eight functional units [19, 20]. Such configurations indicate the presence of clusters which are interpreted in terms of complex defects consisting of Fe ions in an interstitial tetrahedral site with two adjacent octahedral Fe vacancies, which suggest that the foil ferrites are nonstoichiometric oxides in composition. Thus, in foil ferrite samples, their chemical formula can be written as  $\text{Mn}_x\text{Zn}_y\text{Fe}_2\text{O}_4$ , where the Mn cations occupy the tetrahedral sites and the Zn cations occupy the octahedral sites, while  $x$  and  $y$  will be defined as composition parameters [21].

The relative number of planes oriented in a certain direction can be related to the area under the XRD peak, as well as the peak height which will represent that reflection; here XRD is used to determine the orientation corresponding to the significant plane in the foil ferrite structure, being it the  $c$ -axis orientation as the area under the (113) reflection peak. The effect of powder preparation and sintering cycle on the crystal size and thickness in ceramic process technologies for Mn-Zn ferrites is associated with the full width at half maximum (FWHM) and elastic strain ( $\epsilon_{2\theta}$ ) [22].

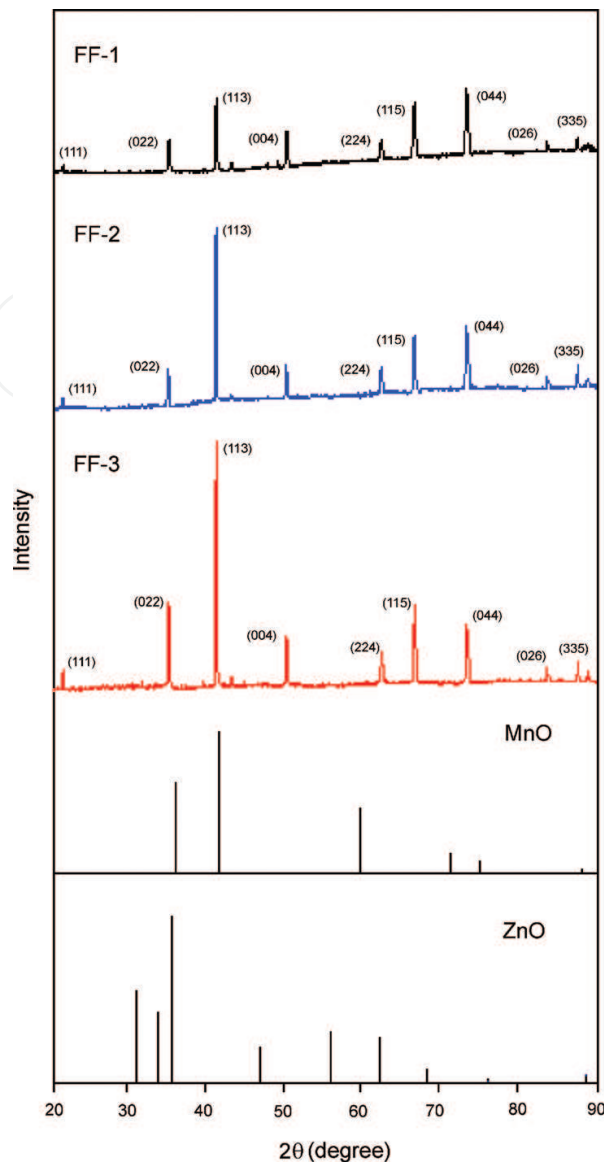


**Figure 3.** XRD patterns of three different foil ferrite samples, where XRD patterns of MnO and ZnO are included as reference for analysis of the strain and chemical composition.

In the case of the foil ferrite irradiated by  $\text{CoK}\alpha$  radiation, the Debye-Scherrer relation becomes  $D = N[(FWHM) \cos\theta]^{-1}$ , where  $D$  is the mean crystallite size,  $N \approx cr$  is the interatomic spacing with  $c = 8.494 \text{ \AA}$  for magnetite,  $r = 0.64 \text{ \AA}$  as the radius of  $\text{Fe}^{+3}$  ion, and  $\theta$  is the reflection angle to the (113) orientation, while the Scherrer relation  $t = \lambda [\epsilon_{2\theta} \cos\theta]^{-1}$ , where  $t$  is the minimum thickness for carrier conduction in the absence of scattering events and  $\epsilon_{2\theta} = (d - d_0)/d$  with  $d$  as the actual atomic plane spacing and  $d_0$  the unstrained atomic plane spacing [23]. **Table 1** gives the structure parameters attained from XRD patterns in foil ferrite samples.

To know the effect of the complex composition of  $\text{Fe}_2\text{O}_3$  mixed with MnO and ZnO on lattice strain, it can be well studied by using  $\frac{\Delta d}{d} = \frac{\Delta\theta}{\tan\varphi}$ , where  $\Delta d/d$  is the average strain along the (113) reflection peak with respect to the substrate,  $\Delta\theta$  as the difference between incident angle for measured (113) plane and the (113) plane corresponding at the magnetite, and  $\varphi$  is the angle with respect to the

Sample	$2\theta$	FWHM	$\epsilon_{2\theta}$	D (nm)	t (nm)
FF-1	40.88°	0.19	$1.22 \times 10^{-4}$	13.34	1565.86
FF-2	40.93°	0.19	$1.07 \times 10^{-3}$	13.35	178.55
FF-3	40.93°	0.19	$1.07 \times 10^{-3}$	13.35	178.55

**Table 1.** Structure parameters in foil ferrites.

substrate planes [24]. As the Mn-Zn ferrite is a powder composition with  $Fe_2O_3$  as their main constituent, a foil ferrite can be approximately seen as a structure MnO/ $Fe_2O_3$ /ZnO where diffusion processes occur; then, for strain analysis the equivalent substrate planes will be both MnO and ZnO as reference XRD patterns (see **Figure 3**) [1]. **Table 2** provides the average strain estimated from XRD patterns in foil ferrite samples.

### 3.2. Electrical analysis

**Figures 4** and **5** explain the measuring strategy to know electrical performance in foil ferrite samples labeled as FF-1, FF-2, and FF-3. Two conditions are performed, both longitudinal and transverse bias as shown in **Figures 4(a)** and **5(a)**, respectively. Current-voltage (I-V) curves are displayed in **Figure 4(b)** at longitudinal bias and at transverse bias in **Figure 5(b)**. Two aluminum electrodes of circular geometry with cross section area of  $3.14 \text{ mm}^2$  are placed on each foil ferrite sample to inject and collect voltage signals. A resistor of  $1 \text{ k}\Omega$  is used to measure the output voltage and thus calculate the current flow by Ohm's law. Ohmic behavior is observed in I-V curves for voltage bias from  $-2$  to  $2 \text{ V}$ , while at higher voltages, I-V curves indicate that current and voltage follow a power-law relationship  $I = \alpha V^n$  with  $n = 1.5$ . Such power-law dependence is characteristic of space-charge-limited conduction (SCLC) [25]. Analysis in I-V curves by using a SCLC model is the experimental method used here with current-voltage dependence proportional to  $\alpha = \frac{9}{8} \epsilon_0 \epsilon_r \mu S L^{-3}$ , where  $\epsilon_0 \epsilon_r$  is the dielectric constant,  $\mu$  is the carrier mobility,  $L$  is the spacing between electrodes, and  $S$  is the cross-sectional area.

Sample	$2\varphi$ (ZnO)	$2\varphi$ (MnO)	$\Delta\theta$	$\left(\frac{\Delta d}{d}\right)_{ZnO}$	$\left(\frac{\Delta d}{d}\right)_{MnO}$
FF-1	34.42°	40.89°	$-5 \times 10^{-3}$	-0.016	-0.013
	62.86°			-0.008	
FF-2	34.42°	40.89°	$44 \times 10^{-3}$	0.14	0.11
	62.86°			0.072	
FF-3	34.42°	40.89°	$44 \times 10^{-3}$	0.14	0.11
	62.86°			0.072	

**Table 2.** Average strain in foil ferrites associated with ZnO and MnO.

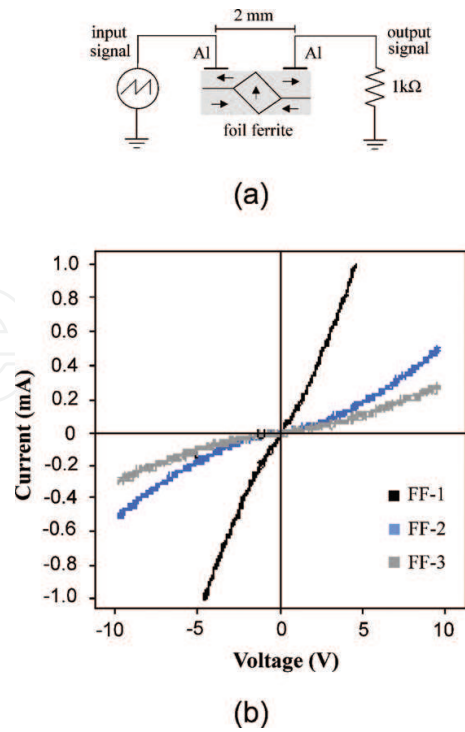


**Figure 4.** (a) Schematic diagram of the foil ferrites in cross-sectional view connected in the test circuit. (b) Current-voltage (I-V) curves of the three different foil ferrite samples, which are longitudinally biased.

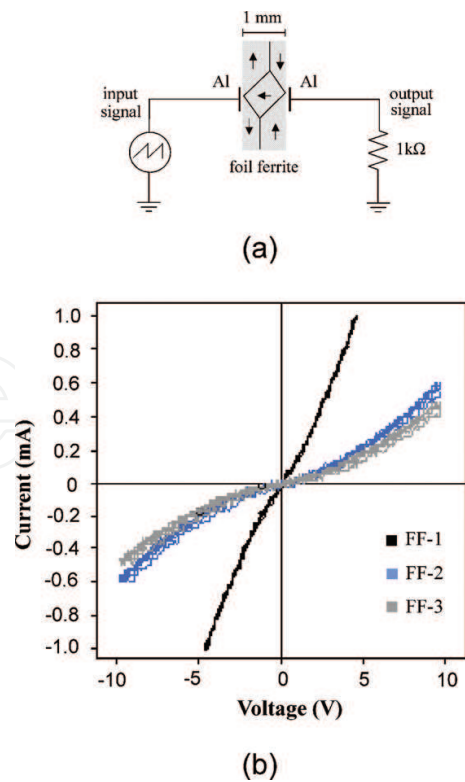


**Figure 5.** (a) Schematic diagram of the foil ferrites in cross-sectional view connected in the test circuit. (b) Current-voltage (I-V) curves of the three different foil ferrite samples, which are transversally biased.

To obtain conduction parameters in foil ferrite samples, the parameter  $\alpha$  was initially calculated from I-V curves. Then, by tracing slopes on I-V curves, the critical voltage,  $V_c = 10enL^2(\epsilon_0\epsilon_r)^{-1}$ , and trap-filled limit voltage,  $V_{TFL} = 6eN_tL^2(\epsilon_0\epsilon_r)^{-1}$ , are found as in earlier methodologies, where both carrier concentration,  $n$ , and trap concentration,  $N_t$ , has been well estimated [26, 27]. Also, adiabatic activation energy,  $\Delta G^*$ , should be responsible for the diffusion processes (displacement reactions) during sintering cycle in processing technology of Mn-Zn bulk ferrites in contrast to the overall activation energy under SCLC. Theoretical studies have reported  $\Delta G^*$  with value of 0.5 eV for pure hematite ( $Fe_2O_3$ ) smaller than the activation energy of about 1 eV at  $T > 800^\circ C$  for conductivity [28]; then as reference  $\Delta G^*$  can be estimated as a function of  $V_c$  for this analysis.

Thus,  $\Delta G^* = 0.5V_c$  will be used to evaluate conduction properties in foil ferrite samples as a function of the mobility  $\mu \sim \exp\left(-\frac{\Delta G^*}{kT}\right)$ , where  $k$  is the Boltzmann constant and  $T$  is equivalent at the processing temperature during sintering cycle. Finally, knowing  $\alpha$  and  $\mu$  parameters,  $\epsilon_0\epsilon_r$  was estimated for both longitudinal and transverse bias. **Table 3** summarizes the conduction parameters at longitudinal bias where  $L = 2$  mm,  $W = 1$  mm (physical width of each foil ferrite under test), and  $S = t \times W$  with  $t$  as the thickness previously estimated by XRD analysis in Section 3.1, while the conduction parameters at transverse bias are registered in **Table 4**, where  $L = 1$  mm and  $S = 3.14 \times 10^{-2} \text{ cm}^2$  is the cross section area of the aluminum electrodes.

Chemical formula  $Mn_xZn_yFe_2O_4$  allows explaining structure and conduction properties in foil ferrites where magnetite  $Fe_3O_4$  is equivalent to  $Fe \cdot Fe_2O_4$  with  $Fe^{+3}$  ion substituted by  $Mn^{+2}$  in the tetrahedral sites and  $Zn^{+2}$  in the octahedral sites. As radius of  $Fe^{+3}$  is smaller than that of  $Zn^{+2}$  and greater than that of  $Mn^{+2}$ , structural disorder will occur; therefore, exchange interactions via the oxygen ions will define magnetic properties as a function of the distance and angle of the Mn—O—Zn bonds; also, SCLC will depend on different conduction mechanisms related to the exponential distribution of defects (grain boundaries) [13, 27]. From results attained here, it is confirmed that the sample FF-1 exhibits lower  $\epsilon_{20}$  than FF-2 and FF-3 samples. Chemical composition approximately proportional to the average strain ( $x \sim \left(\frac{\Delta d}{d}\right)_{MnO}$  and  $y \sim \left(\frac{\Delta d}{d}\right)_{ZnO}$ ) in samples FF-2 and FF-3 resulted to be positive associated to tensile stress while negative in sample FF-1 related to compressive stress. In the samples,  $x$  and  $y$  are connected by the coupling type dominant in the Mn—O—Zn bonds, where tensile stress dominated by longer distance and angle of  $180^\circ$  is *antiferromagnetically coupled*, while compressive stress is *ferromagnetically coupled* at shorter distance with angle of  $90^\circ$ . The  $V_c$  and  $V_{TFL}$  voltages from **Tables 3** and **4** were extracted to evaluate the charge concentration (carrier distribution), resulting  $n$  in the range from  $10^{20}$  to  $10^{22} \text{ cm}^{-3}$  at the surface while  $N_t$  in the range from  $10^{15}$  to  $10^{17} \text{ cm}^{-3}$  at the bulk of each sample, which reveals that major differences of  $\epsilon_0\epsilon_r$  and magnetic ordering are correlating to the charge concentration differences of foil ferrites.

Sample	$\alpha$	$V_c$ (V)	$\Delta G^*$ (eV)	$V_{TFL}$ (V)	$\mu$ ( $\text{cm}^2 \text{V}^{-1} \text{s}^{-1}$ )	$\epsilon_0\epsilon_r$ ( $\text{F cm}^{-1}$ )
FF-1	$0.92 \times 10^{-4}$	1.12	0.56	2.32	$5.49 \times 10^{-3}$	7.61
FF-2	$1.32 \times 10^{-5}$	1.44	0.72	2.88	$1.43 \times 10^{-3}$	36.87
FF-3	$0.85 \times 10^{-5}$	1.68	0.84	2.64	$4.83 \times 10^{-4}$	632.74

**Table 3.** Conduction parameters at longitudinal bias.

Sample	$\alpha$	$V_C$ (V)	$\Delta G^*$ (eV)	$V_{TFL}$ (V)	$\mu$ ( $cm^2 V^{-1} s^{-1}$ )	$\epsilon_0 \epsilon_r$ ( $F cm^{-1}$ )
FF-1	$0.92 \times 10^{-4}$	1.12	0.56	2.32	$5.49 \times 10^{-3}$	$4.74 \times 10^{-4}$
FF-2	$1.82 \times 10^{-5}$	1.28	0.64	2.42	$2.97 \times 10^{-3}$	$1.73 \times 10^{-4}$
FF-3	$0.48 \times 10^{-5}$	1.12	0.56	2.56	$5.49 \times 10^{-3}$	$2.47 \times 10^{-5}$

Table 4. Conduction parameters at transverse bias.

## 4. Foil ferrite as functional green device

This section discusses the possibility of the functional green devices built by foil ferrite samples. Electrical performance under both longitudinal and transverse bias conditions has confirmed nonlinear behavior which obeys at the conduction properties through orderly small grained structure being it equivalent to the magnetic-electrical conduct of a self-inductor with hysteresis when it is connected as shown in **Figure 6**. Current-voltage (I-V) curves are obtained by using a digital storage oscilloscope (Tektronix, TDS1012C) at room temperature. A function generator (Matrix, MFG-8250A) was used to produce the input voltage signals.

To connect the input signal and collect the output signal in the applications shown here, two aluminum electrodes of circular geometry with cross section area of  $0.1 \times 0.1 \text{ cm}^2$  have been placed on each foil ferrite; also, a resistor has been used to measuring of the output signals.

### 4.1. Mixer circuit

Modulation is the process of converting information one wants to obtain into one or more properties of a sinusoidal signal called the carrier. This information can be analogic signal, such as a varying voltage or current, or a digital signal, which consists of sequence of bits, i.e., 0 and 1 values. In general several modulation schemes can be represented by using mixer circuits. The main type of modulator recently employed is the quadrature mixer [29].

To disclose the performance of a foil ferrite as mixer circuit to modulation process, a basic schematic diagram of **Figure 7** has been built. A full-rectified signal with amplitude of 15 V was applied on first outer node at operating frequency of 120 Hz. In the middle node, a sinusoidal signal with amplitude of  $\pm 7.5 \text{ V}$  at operating frequency of 500 Hz was applied. The full-rectified signal was obtained by a variable self-transformer of alternating voltage from 0 to 150 V. A resistor of 1 k $\Omega$  is connected in the second outer node to monitoring of mixing signal (see **Figure 7**). It is observed that the mixing signal follows the shape of the full-rectified signal when it is larger than the sinusoidal signal, producing an output signal with amplitude of  $\pm 3.5 \text{ V}$ . Otherwise, when the amplitude of the sinusoidal signal is greater with respect to the full-rectified signal, mixing process is negligible, because there are strong anisotropy differences among longitudinal and transverse paths on foil ferrite samples related to its structural disorder. Therefore, a foil ferrite will operate in the electronic signal processors integrated by mixer circuits to drive control systems as a function of complex signals at low-power excitation [30].

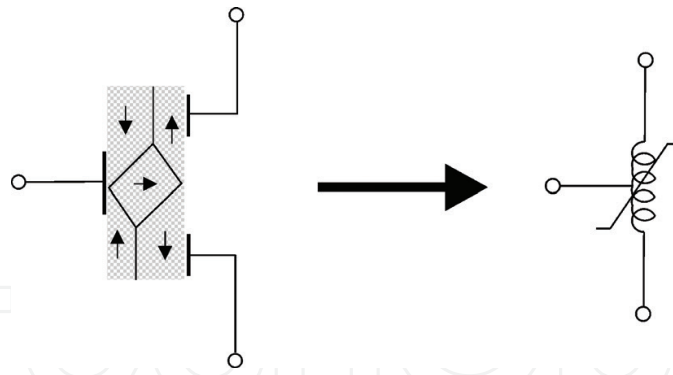


Figure 6. Foil ferrite equivalent at the self-inductor with hysteresis.

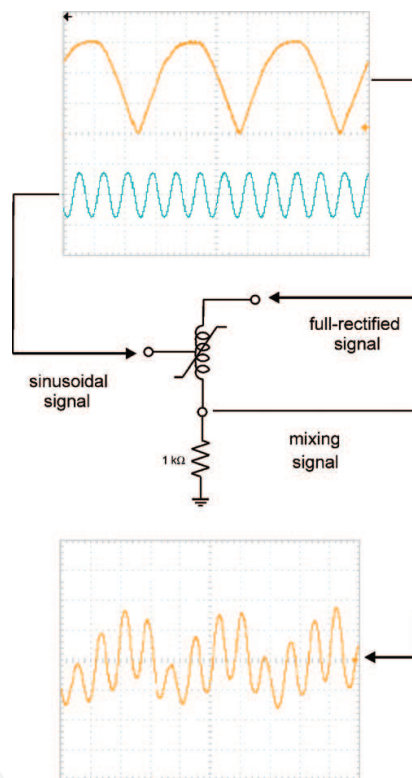
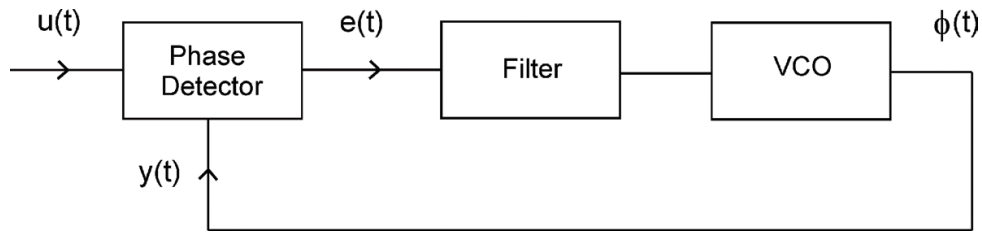


Figure 7. Schematic of the mixer circuit done with foil ferrite FF-1 when it is operating under full-rectified and sinusoidal signals to produce mixing signal.

#### 4.2. Phase detector

A phase detector produces a voltage proportional to  $e(t) = u(t) - y(t)$  as the phase difference between the signals  $u(t)$  and  $y(t)$  in the block diagram of **Figure 8**. This block diagram corresponds to phase-locked loop (PLL) system. A PLL is comprised of three blocks: phase detector, filter, and voltage-controlled oscillator (VCO).

The voltage  $e(t)$  upon filtering is used as control signal for the VCO. The VCO produces a frequency proportional to input signal  $u(t)$ , and any time variant signal appearing on the filter output will modulate the VCO frequency [31]. A feedback path among VCO and phase detector



**Figure 8.** Block diagram of a conventional phase-locked loop (PLL) system.

produces unity gain, and as a result, the PLL provides an online estimate of the synchronized fundamental component,  $y(t)$ , and its phase angle,  $\phi(t)$ , with output frequency equal to that of the input during phase lock. The PLL is an adaptive system which follows variations in amplitude, phase angle, and frequency of signal  $u(t)$ . Hence, the structure of a PLL is simple, and this makes it suitable for real-time applications for hardware implementations [32].

The schematic circuit of **Figure 9** was used to evaluate the performance of the foil ferrite sample as phase detector. A resistor of  $10\text{ k}\Omega$  is connected in node  $v_0$  to monitoring of output signal. To simulate phase difference between two sinusoidal signals, a low-pass filter built with a simple RC circuit was implemented [33]. Signal connected to the RC circuit input relates  $v_1$ , while signal collected from RC circuit matches with  $v_2$ . Such signals are applied on nodes  $v_1$  and  $v_2$  where  $\pm 10\text{ V}$  is fixed in  $v_1$  at operating frequency in the range of 0.5 to 5 kHz. The resulting waveforms are shown from **Figure 10(a)–(c)**.

At 0.5 kHz, the phase angle between signals  $v_1$  and  $v_2$  is  $22.5^\circ$ , while to 1 kHz is  $40.5^\circ$  and when operating frequency increase until 5 kHz resulted to be  $58.5^\circ$ . Meanwhile, at the output node  $v_0$ , when frequency is 0.5 kHz, 1 kHz, and 5 kHz, the phase angle corresponds to  $4.5^\circ$ ,  $9.2^\circ$ , and  $1.2^\circ$ , respectively. It is observed that the phase angle between  $v_0$  and  $v_1$  signals is close to zero when phase angle between  $v_1$  and  $v_2$  signals shift from 0 to  $90^\circ$ .

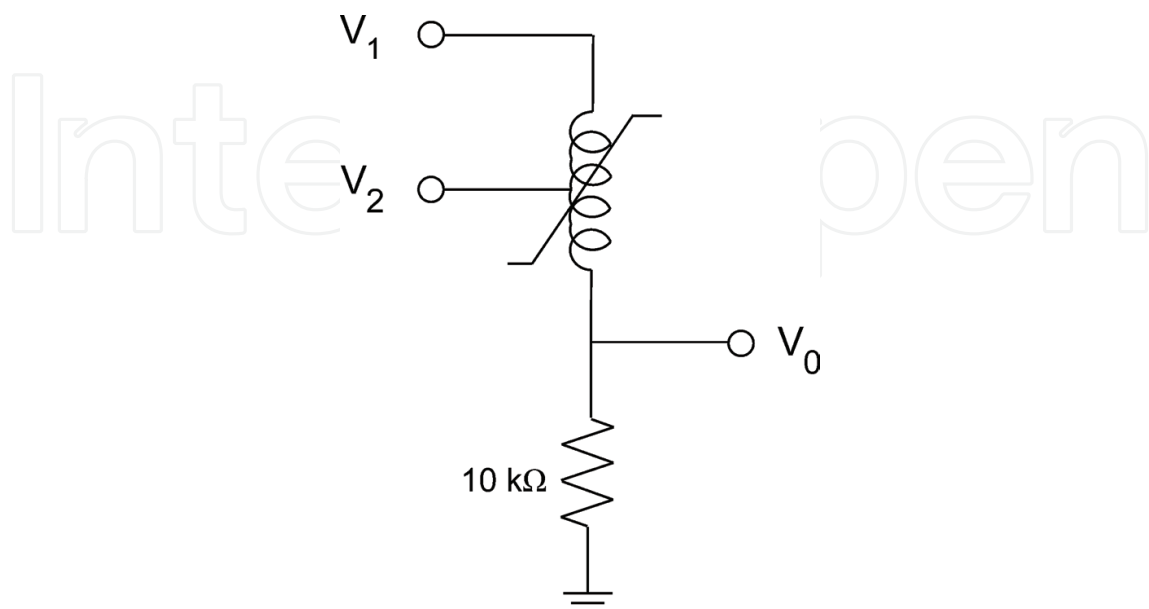


**Figure 9.** Schematic circuit to evaluate the performance of the foil ferrite FF-3 as phase detector.

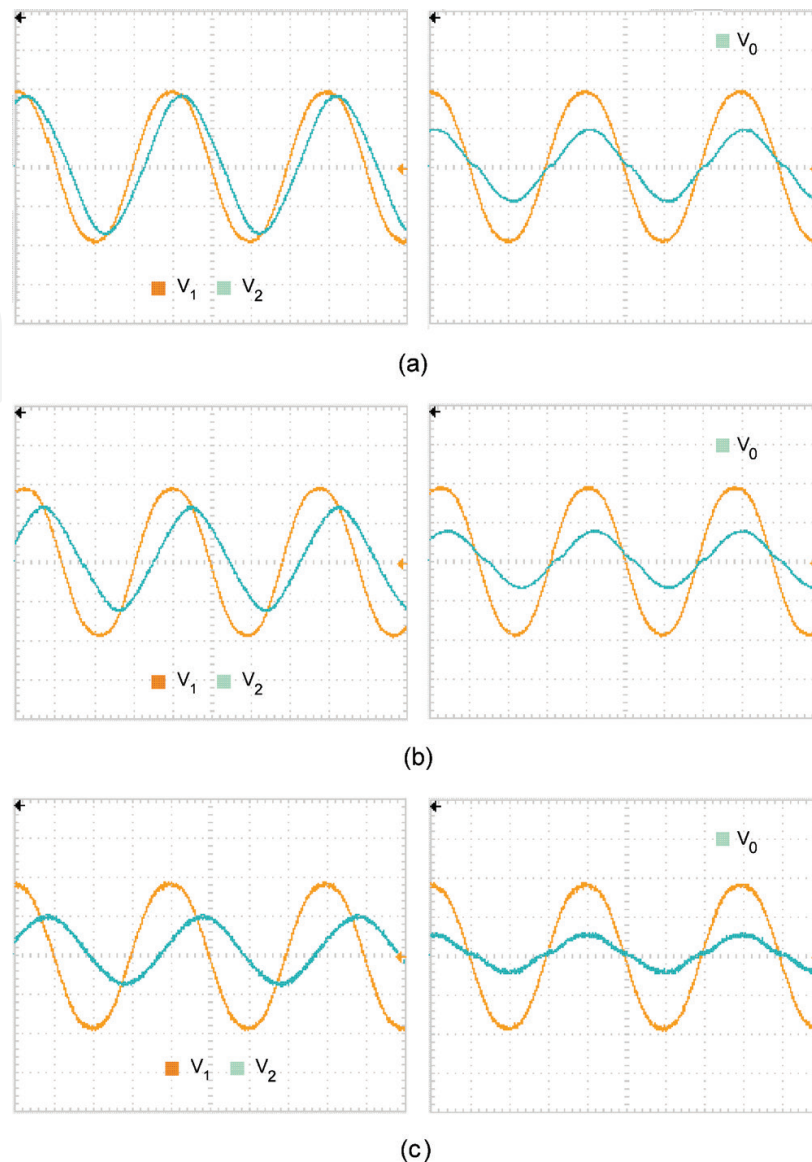


**Figure 10.** Waveforms monitored from the schematic circuit of **Figure 9** driven at three operating frequencies: (a) 0.5, (b) 1, and (c) 5 kHz. The input and output signals are shown.

Also,  $V_2$  and  $V_0$  signals decrease slowly as frequency rises. Results from **Figure 10** indicate that foil ferrite samples of grain-reduced crystalline structure with single magnetic domain offer controllable power losses under low-frequency excitation. Hence, a foil ferrite will operate like PLL system.

## 5. Summary

Since 1994, initiatives in response to the environmental and ecotoxicological concerns in manufacturing processes based on life-cycle assessment (LCA) have been established. To manufacturing electronic devices with desired characteristics, the conventional selection of raw materials had depended on link between material and function; however, environmental consequences of

use, availability, and recycling have not been taken into account. Nevertheless, to ensure availability of the materials for future generations, the transformation of waste into usable materials has been discussed here, as more environmentally beneficial which implies that resource disposal and material flow will require well-designed systems into manufacturing stages. The latter is a challenge for engineers and scientists responsible with the current state of the nature resources.

The Mn-Zn ferrites have been chosen as recycled material resource because it provides suitable uncommon physical properties when it is converted from bulk ferrite to foil ferrite. Also, negative environmental impact such as emission of toxic gases during powder preparation, higher use of energy resources into sintering cycle, and electronic waste from consumer electronics has demonstrated that Mn-Zn ferrites in bulk shape take their final placement often in landfills. But, to take advantages of the properties in foil ferrites, a recycling model has been employed here as a methodology based on Life-Cycle Green Strategy (LCGS) to ensure recycling efficiency during all overall stages into the green manufacturing.

Due to the interrelation of the structure and conduction properties as a function on magnetic ordering which is the key issue in green electronic device design, the x-ray diffraction and electrical studies have been done on foil ferrites to know if the operating parameters are useful and when it would be used as functional green device. Those studies have confirmed that structural disorder and carrier concentration under longitudinally and transversally bias conditions are responsible of the nonlinear behavior which obeys at the carriers' conduction into their small grained crystalline structure.

Finally, it has been shown that fundamental tools such as recycling practices and basic characterization routes are needed to provide theoretical basis for the green materials exploration, converting waste materials into suitable materials in its second life. Discovering the fascinating properties of the materials, especially structure, conduction, and magnetic parameters is a key to continue the trends to green processing and then synthesize adaptive oxide materials intended for electronic signal processors.

## Author details

Roberto Baca

Address all correspondence to: [rbaca02006@yahoo.com.mx](mailto:rbaca02006@yahoo.com.mx)

Department of Electronics, National Polytechnic Institute, México City, Mexico

## References

- [1] Grove AS. Physics and Technology of Semiconductors Devices. 1st ed. United States of America: John Wiley & Sons; 1972. 357 p
- [2] Keyser CA. Materials Science in Engineering. 6th ed. United States of America: Prentice-Hall, Inc; 1972. 460 p

- [3] Ogunseitan OA, Schoenung JM. Human health and ecotoxicological considerations in materials selection for sustainable development. *Materials Research Bulletin*. 2012;**37**:356-363. DOI: 10.1557/mrs.2012.8
- [4] Shamaila S, Leghari Saijad AK, Ryma N-ul-A, Anis Farooqi S, Jabeen N, Majeed S, et al. Advancements in nanoparticle fabrication by hazard free eco-friendly green routes. *Applied Materials Today*. 2016;**5**:150-199. DOI: 10.1016/j.apmt.2016.09.009
- [5] Nakamura S. Current Status of GaN-Based solid state lighting. *Materials Research Bulletin*. 2009;**34**:101-107
- [6] Baca R, Cheong KY. Green synthesis of iron oxide thin-films grown from recycled iron foils. *Materials Science in Semiconductor Processing*. 2015;**29**:294-299. DOI: 10.1016/j.mssp.2014.05.014
- [7] Díaz Coutiño R. *Desarrollo Sustentable*. 2nd ed. Mexico: McGraw-Hill/INTERAMERICANA EDITORES; 2011. 305 p
- [8] Reuter M, Van Schaik A. Opportunities and limits of recycling. A dynamic-model-based analysis. *Materials Research Bulletin*. 2012;**37**. DOI: 10.1557/mrs.2012.57
- [9] Lee J-P, Kim JH, Pyo Chae K, Bae-Lee Y. Crystallographic and magnetic properties of Zn-Mn ferrite. *Journal of the Korean Physical Society*. 2006;**49**(2):604-607
- [10] Magnetic Materials Producers Association. *Soft Ferrites. A User's Guide* [Internet]. 1998. Available from: <http://www.google.com/mmpa/SFG-98.pdf>
- [11] Zvezdin AK, Kostyuchenko VV. Magnetic-field-induced phase transitions in molecular ferrimagnets with two compensation points. *Physics of the Solid State*. 2001;**43**(9): 1715-1719
- [12] Tian G-S, Lin H-Q. Phase transition and ferrimagnetic long-range order in the mixed-spin Heisenberg model with single-ion anisotropy. *Physical Review*. 2004;**70**:104412
- [13] Blundell S. *Magnetism in Condensed Matter*. 2nd ed. Great Britain: Oxford University in Press; 2008. 234 p
- [14] Fiorillo F. DC and AC magnetization processes in soft magnetic materials. *Journal of Magnetism and Magnetic Materials*. 2002;**242-245**
- [15] Verma A, Alam MI, Chatterjee R, Goel TC, Mendiratta RG. Development of a new soft ferrite core for power applications. *Journal of Magnetism and Magnetic Materials*. 2006;**300**. DOI: 10.1016/j.jmmm.2005.05.040
- [16] Chan Samuel SM, Chung Henry SH, Hui Ron SY. Self-oscillating dimmable electronic ballast for fluorescent lamps. *IEEE Power Electronics Letters*. 2004;**2**(3):87-91. DOI: 10.1109/LPEL.2004.838777
- [17] Cao J, Wu J. Strain effects in low-dimensional transition metal oxides. *Materials Science and Engineering R*. 2011;**71**. DOI: 10.1016/j.mser.2010.08.001
- [18] Khalil HK. *Nonlinear Systems*. 1st ed. United States of America: Macmillan Publishing Company; 1992. 564 p

- [19] Hamdeh HH, Ho JC, Oliver SA, Willey RI, Oliveri G, Busca G. Magnetic properties of partially-inverted zinc ferrite aerogel powders. *Journal of Applied Physics*. 1997;**81**. DOI: 10.1063/1.364068
- [20] Wang Z, Schiferl D, Zhao Y, O'Neill HStC. High pressure Raman spectroscopy of spinel-type ferrite  $ZnFe_2O_4$ . *Journal of Physics and Chemistry of Solids*. 2003;**64**:2517-2523. DOI: 10.1016/j.jpcs.2003.08.005
- [21] Kundaliya DC, Ogale SB, Lofland SE, Dhar S, Metting CJ, Shinde SR, et al. On the origin of high-temperature ferromagnetism in the low-temperature processed Mn-Zn-O system. *Nature Materials*. 2004;**3**:709-714. DOI: 10.1038/nmat.1221
- [22] Wang C, Chen Z, He Y, Li L, Zhang D. Structure, morphology properties of Fe-doped ZnO films prepared by facing-target magnetron sputtering system. *Applied Surface Science*. 2009;**255**:6881-6887. DOI: 10.1016/j.apsusc.2009.03.008
- [23] Fewster PF. *X ray Scattering from Semiconductors*. 2nd ed. Great Britain: Imperial College Press; 2003. 299 p
- [24] Baca-Arroyo R. Structural characterization of the chromium-iron alloy formed by thermal diffusion processes. *Advances Materials Research*. 2013;**651**:284-288. DOI: 10.4028/www.scientific.net/AMR.651.284
- [25] Grinberg AA, Luryi S, Pinto MR, Schryer NL. Space-charge-limited current in a film. *IEEE Transactions on Electron Devices*. 1989;**36**(6):1162-1170
- [26] Xu W, Chin A, Ye L, Ning CZ, Hu H. Charge transport and trap characterization in individual GaSb nanowires. *Journal of Applied Physics*. 2012;**111**:104515. DOI: 10.1063/1.4720080
- [27] Baca-Arroyo R. Nonlinear-electronic transport in  $Fe_2O_3$  thin films grown from grain-oriented iron foils. *Advances in Materials Science and Engineering*. 2013;**2013**:987572
- [28] Liao P, Caspary Toroker M, Carter EA. Electron transport in pure and doped hematite. *Nanoletters*. 2011;**11**:1775-1781. DOI: 10.1021/nl200356n
- [29] Aidin Bassan S, Chen W, Helaoui M, Ghannouchi FM. Transmitter architecture for CA. *IEEE Microwave Magazine*. 2013;**14**(15):78-86. DOI: 10.1109/MMM.2013.2259399
- [30] Terrovitis MT, Meyer RG. Intermodulation distortion in current-commutating CMOS Mixers. *IEEE Journal of Solid-State Circuits*. 2000;**35**(10):1461-1473
- [31] Zhao B, Mao X, Yang H, Wang H. A voltage-controlled oscillator with an ultra-low supply voltage and its application to a fractional-N phase-locked loop. *International Journal of Electronics*. 2009;**96**(10):1012-1022
- [32] Karimi-Ghartermani M, Mokhtari H, Reza Iravani M, Sedighy M. A signal processing system for extraction of harmonics and reactive current of single-phase systems. *IEEE Transactions on Power Delivery*. 2004;**19**(3)
- [33] Sedra AS, Smith KC. *Microelectronic Circuits*. 4th ed. United States of America: Oxford University in Press; 1998. 1400 p

